Original Article

The clinical, radiological, postoperative pathological, and genetic features of nodular lung adenocarcinoma: a real-world single-center data

Weixiang Zhong[1,2]^, Wenshu Zhang[3], Lei Dai[4], Mingwu Chen[1,4]

[1]First Clinical Medical College, Guangxi Medical University, Nanning, China; [2]Department of Thoracic Surgery, the First Affiliated Hospital of Gannan Medical University, Ganzhou, China; [3]Department of Pathology, the First Affiliated Hospital of Gannan Medical University, Ganzhou, China; [4]Department of Cardiothoracic Surgery, the First Affiliated Hospital of Guangxi Medical University, Nanning, China

Contributions: (I) Conception and design: W Zhong, M Chen; (II) Administrative support: M Chen; (III) Provision of study materials or patients: W Zhong; (IV) Collection and assembly of data: W Zhong, L Dai; (V) Data analysis and interpretation: W Zhong, W Zhang, L Dai; (VI) Manuscript writing: All authors; (VII) Final approval of manuscript: All authors.

Correspondence to: Mingwu Chen, MD. First Clinical Medical College, Guangxi Medical University, No. 22 Shuangyong Road, Nanning 530021, China; Department of Cardiothoracic Surgery, the First Affiliated Hospital of Guangxi Medical University, No. 6 Shuangyong Road, Nanning 530021, China. Email: chen535@126.com.

Background: The preoperative differential diagnosis of nodular lung adenocarcinoma has long been a challenging issue for thoracic surgeons. This study aimed to explore differential diagnosis of nodular lung adenocarcinoma by comprehensively analyzing its clinical, computed tomography (CT) imaging, and postoperative pathological and genetic features.

Methods: The clinical, CT imaging, and postoperative pathological features of different classifications of nodular lung adenocarcinoma were retrospectively analyzed through univariate and multivariate statistical methods.

Results: There were 132 patients with nodular lung adenocarcinoma enrolled. Firstly, compared with ground-glass nodular lung adenocarcinoma, solid nodular lung adenocarcinoma was more common in women [odds ratio (OR), 3.662; 95% confidence interval (CI): 1.066–12.577] and older adults (OR, 1.061; 95% CI: 1.007–1.119), and CT signs were mostly lobulation (OR, 4.957; 95% CI: 1.714–14.337) and spiculation (OR, 8.214; 95% CI: 2.740–24.621); the mean CT (CT_m) value of solid nodular lung adenocarcinoma was significantly higher than that of ground-glass nodular lung adenocarcinoma, and the optimal diagnostic threshold was –267.5 Hounsfield units (HU). Secondly, the maximum diameter of nodule size (NS_{max}) of invasive adenocarcinoma (IAC) was significantly greater than that of minimally IAC (MIA; OR, 6.306; 95% CI: 1.191–33.400) or atypical adenomatous hyperplasia (AAH)/adenocarcinoma in situ (AIS; OR, 189.539; 95% CI: 4.720–7,610.476), and the optimal diagnostic threshold between IAC and MIA was 1.35 cm; the CT_m value of IAC was significantly higher than that of MIA, and the optimal diagnostic threshold was –460.75 HU. Thirdly, lepidic-predominant adenocarcinoma (LPA) manifest more commonly as pure ground-glass nodule (pGGN; OR, 6.252; 95% CI: 1.429–27.358) or mixed ground-glass nodule (mGGN; OR, 4.224; 95% CI: 1.223–14.585). Moreover, the mutation rate of epidermal growth factor receptor (*EGFR*) in IAC was 70.69% (41/58). The *EGFR* mutation rates of mGGNs (OR, 8.794; 95% CI: 1.489–51.933) and solid nodules (SNs; OR, 12.912; 95% CI: 1.597–104.383) were significantly higher than that of pGGNs. Furthermore, compared with those of micropapillary-predominant adenocarcinoma (MPA), solid-predominant adenocarcinoma (SPA), or invasive mucinous adenocarcinoma (IMA), there were significantly higher *EGFR* mutation rates in acinar-predominant adenocarcinoma/papillary-predominant

^ ORCID: 0000-0003-2673-227X.

adenocarcinoma (APA/PPA; OR, 55.925; 95% CI: 4.045–773.284) and LPA (OR, 38.265; 95% CI: 2.307–634.596).

Conclusions: Different classifications of nodular lung adenocarcinoma have their own clinicopathological and CT imaging features, and the latter is the main predictor.

Keywords: Ground-glass nodule (GGN); solid nodule (SN); nodular lung adenocarcinoma; invasive adenocarcinoma (IAC)

Submitted Mar 27, 2024. Accepted for publication May 11, 2024. Published online May 21, 2024.
doi: 10.21037/jtd-24-510
View this article at: https://dx.doi.org/10.21037/jtd-24-510

Introduction

Globally, lung cancer is the most common cause of cancer mortality in men and, after breast cancer, the second leading cause of cancer-related death in women (1). The epidemiological data for malignant tumors (2) in China indicate that the lung cancer incidence (57.26/100,000) and mortality (45.87/100,000) are first among all domestic malignant tumors, and the overall 5-year survival rate of patients is only 19.7%. This can be attributed to the fact that 75% of patients are diagnosed with advanced lung cancer at the time of diagnosis and thus may miss the most opportune window for radical treatment (3).

Highlight box

Key findings

- Solid nodular lung adenocarcinoma is more common in relatively older women, and its mean computed tomography (CT_m) is significantly higher than that of ground-glass nodular lung adenocarcinoma; the maximum diameter of nodule size and CT_m values of invasive adenocarcinoma were significantly higher than those of minimally invasive adenocarcinoma or atypical adenomatous hyperplasia/adenocarcinoma in situ, and lepidic-predominant adenocarcinoma was mostly ground-glass nodule on chest CT images.

What is known and what is new?

- It has been reported that pleural retraction sign, lobulation sign, and spiculation sign are typical CT signs of lung cancer.
- We report that the size, density, and CT_m value of the nodule, along with lobulation sign and spiculation sign can be predictive of different classifications of nodular lung adenocarcinoma.

What is the implication, and what should change now?

- In clinical practice, the preoperative differential diagnosis of nodular lung adenocarcinoma mainly depends on its CT imaging features, especially the size, density, CT_m value of the nodule, lobulation sign and spiculation sign.

Thanks to the spread of low-dose computed tomography (LDCT) in lung cancer screening, the detection rate of asymptomatic pulmonary nodules, especially ground-glass nodules (GGNs), is increasing, about 5% GGNs may eventually develop into lung cancer (4). Yang *et al.* (5) demonstrated that LDCT screening can detect up to 94.1% of early lung cancers and can increase the diagnostic rate of early lung cancer in high-risk groups by 74.1%. The 10-year disease-specific survival rates of adenocarcinoma in situ (AIS) and minimally invasive adenocarcinoma (MIA) with early diagnosis and complete resection are 100% and 100%, respectively (6). In contrast, the 5-year cumulative recurrence rate of stage I invasive adenocarcinoma (IAC) after complete resection is as high as 24.5% (7). Therefore, early detection, diagnosis, and treatment are the keys to improving the survival rate and reducing the mortality of lung cancer.

The preoperative differential diagnosis of malignant pulmonary nodules, especially GGNs, has consistently been a challenge for thoracic surgeons. In clinical practice, computed tomography (CT) imaging features of nodules constitute the main means to discriminating malignant from benign pulmonary nodules, with pleural retraction sign, lobulation sign, and spiculation sign being the typical CT signs of lung cancer (8,9). Numerous studies (8,10-13) have been conducted concerning the clinical, imaging, and pathological features of early lung adenocarcinoma, yet there are spare reports on the different subgroups of nodular lung adenocarcinoma. In this real-world, single-center retrospective study, univariate and multivariate statistical methods were used to comprehensively analyze the differences in the clinical, CT imaging, and postoperative pathological features of patients with different subtypes of nodular lung adenocarcinoma. Additionally, we sought to further elucidate the molecular genetic profile of IAC in order to inform the early differential diagnosis of

nodular lung adenocarcinoma. We present this article in accordance with the STROBE reporting checklist (available at https://jtd.amegroups.com/article/view/10.21037/jtd-24-510/rc).

Methods

The study was conducted in accordance with the Declaration of Helsinki (as revised in 2013). The study was approved by the Ethics Committee of the First Affiliated Hospital of Gannan Medical University (No. LLSC-2022111603), and informed consent was taken from all the patients.

Participants

The total number of patients with pulmonary nodule admitted to the Department of Thoracic Surgery of the First Affiliated Hospital of Gannan Medical University and underwent surgical resection during February 2022 to April 2023 was 190. The number of patients admitted during the study period determined the sample size.

According to the Chinese expert consensus on the diagnosis and treatment of pulmonary nodules, we routinely performed CT follow-up for the first discovered pulmonary nodules, with the follow-up frequency 3 to 12 months. The longest follow-up period of this study was more than 3 years, and of course, there were some patients who directly chose surgical resection due to excessive anxiety.

The following inclusion criteria were applied to screen patients: (I) age ≥18 years old; (II) chest CT signs including solitary or multiple pulmonary GGNs or solid nodules (SNs) with nodule size ranging from 5 to 30 mm but no hilar or mediastinal lymph node enlargement or distant lymph node metastasis; (III) benign or malignancy pulmonary nodules confirmed via postoperative pathological examination, lung primary adenocarcinomas was confirmed on microscopy and tumor features were further evaluated; (IV) complete chest CT images, clinical records, and postoperative pathological data; and (V) newly diagnosed malignancy with no history of chemotherapy, targeted therapy, immunotherapy, radiofrequency ablation, or other antitumor treatments.

Meanwhile, the exclusion criteria were as follows: (I) no chest CT image data from our hospital before operation and no possibility for follow-up or evaluation; (II) CT signs of pulmonary nodules indicating hilar or mediastinal lymph node enlargement or distant lymph node metastasis; and (III) administration of antitumor treatments before surgery, such as chemotherapy, targeted therapy, immunotherapy, and radiofrequency ablation.

Procedure

Differences in the clinical and CT imaging features between benign and malignant pulmonary nodules

All chest CT scans were reconstructed and archived with 1.25 mm contiguous thin sections to enable accurate characterization and measurement of pulmonary nodules. Chest CT scan conditions: voltage 100 kV; current 100–500 SmartmA; noise index: 11.0. Primary scanning parameters were set as follows: scanner field of view (SFOV): large body; display field of view (DFOV): 32 cm; pitch: 0.992:1; slice thickness: 5.0 mm; interval: 5.0 mm; window width: 1,500 Hounsfield units (HU); window level: −700 HU; recon type: lung.

The clinical features included gender, age, smoking history, and personal and family history of cancer, with smoking being defined as a cumulative minimum of 100 cigarettes.

The imaging features of chest CT including site, number, size, density, and mean CT (CT_m) value of pulmonary nodules, pleural retraction sign, lobulation sign, spiculation sign, vacuole sign, and air bronchogram sign, were analyzed by senior doctors with experience in chest CT diagnosis, as shown in *Figure 1*.

In this study, the size of pulmonary nodule was confirmed by measuring the maximum diameter of nodule size (NS_{max}) at the lung window level of chest CT. The region of interest (ROI) was manually delineated on the maximum diameter of the pulmonary nodule under the chest CT lung window to measure the CT_m value. A polygonal or circular ROI was selected according to the shape of the lesion to avoid blood vessels, bronchi, vacuoles, and other structures, with three different positions being measured and the average value being recorded, as shown in *Figure 2*.

Nodular lung adenocarcinoma and its subgroup classification

According to the 2021 World Health Organization (WHO) classification of lung tumors, we refer to atypical adenomatous hyperplasia (AAH)/AIS or MIA or IAC that appear as GGNs or SNs on chest CT images as nodular lung adenocarcinoma. Subgroup classification was performed according to nodule density, postoperative pathological type, and grade. The clinical, CT imaging, and pathological features of each subgroup of nodular lung

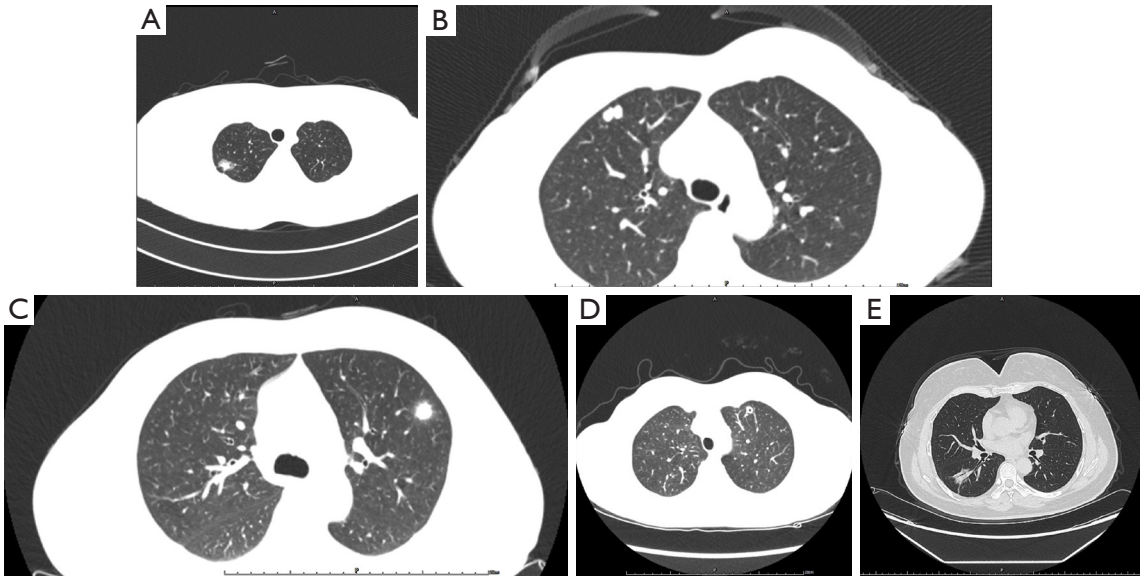

Figure 1 Common chest CT signs of pulmonary nodules. (A) Pleural retraction sign; (B) lobulation sign; (C) spiculation sign; (D) vacuole sign; (E) air bronchogram sign. CT, computed tomography.

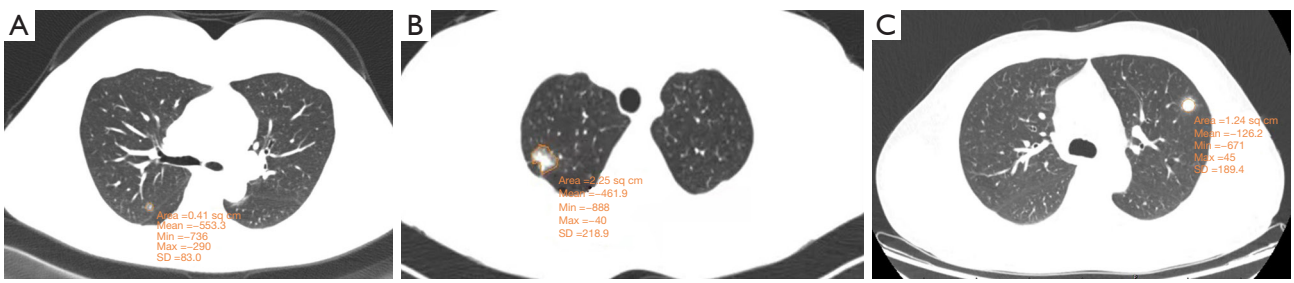

Figure 2 Measurement of CT_m value of pulmonary nodules (unit: HU). (A) CT_m value of pGGN; (B) CT_m value of mGGN; (C) CT_m value of SN. SD, standard deviation; CT_m, mean computed tomography; HU, Hounsfield units; pGGN, pure ground-glass nodule; mGGN, mixed ground-glass nodule; SN, solid nodule.

adenocarcinoma were further analyzed via univariate and multivariate statistical analyses.

According to the density of the nodule, nodular lung adenocarcinoma was classified as ground-glass nodular lung adenocarcinoma and solid nodular lung adenocarcinoma. Moreover, according to the postoperative pathological type, it was classified as AAH/AIS, MIA, and IAC.

According to the postoperative pathological grading system of IAC (14), IAC was classified as lepidic-predominant adenocarcinoma (LPA), acinar-predominant adenocarcinoma (APA)/papillary-predominant adenocarcinoma (PPA), and micropapillary-predominant adenocarcinoma (MPA)/solid-predominant adenocarcinoma (SPA)/invasive mucinous adenocarcinoma (IMA), as shown in *Figure 3*.

Postoperative pathological features, including pathological types and subtypes, tumor size (pT), lymph node (pN), spread through air spaces (STAS), lymphovascular invasion (LVI), and nerve invasion (NI), were reviewed by senior doctors with experience in the pathological diagnosis of chest tumors (*Figure 4*).

Genetic test in IAC

The recommended targeted genes of non-small cell lung cancer (NSCLC) were detected via next-generation sequencing (NGS) based on Illumina sequencing platform in lung tissue samples of IAC after surgery. The molecular gene mutation spectrum of IAC and its clinical, imaging,

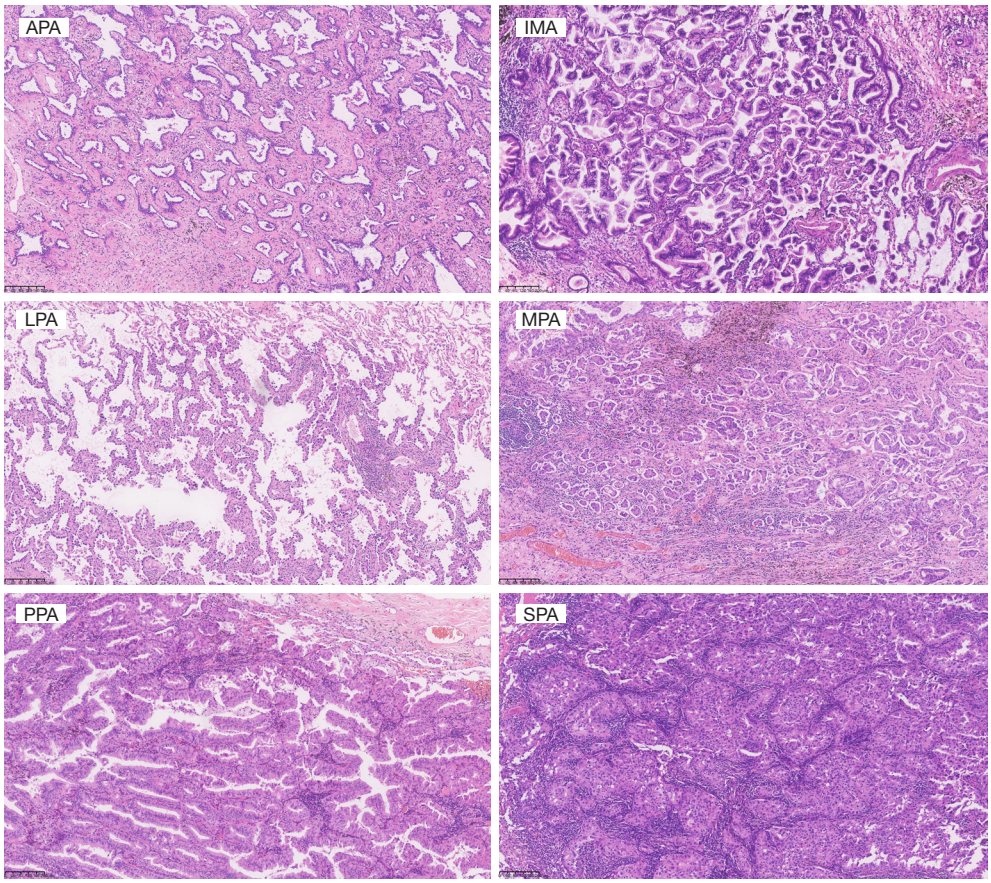

Figure 3 Pathological classification of IAC (hematoxylin-eosin staining, 10× magnification power). APA, acinar-predominant adenocarcinoma; IMA, invasive mucinous adenocarcinoma; LPA, lepidic-predominant adenocarcinoma; MPA, micropapillary-predominant adenocarcinoma; PPA, papillary-predominant adenocarcinoma; SPA, solid-predominant adenocarcinoma; IAC, invasive adenocarcinoma.

and pathological features were further statistically analyzed.

Sample preparation

For specimen fixation, 58 postoperative lung tissue samples of IAC were fixed via paraffin embedding in the Department of Pathology of the First Affiliated Hospital of Gannan Medical University, and 15 pathological white slices were cut to least a 5-μm thickness and sent to a third-party testing agency for NGS detection.

The detection of targeted genes in IAC

The recommended molecular gene mutation profiles of NSCLC, including epidermal growth factor receptor (*EGFR*) mutation, echinoderm microtubule-associated protein like 4-anaplastic lymphoma kinase (*EML-ALK*) rearrangement, Kirsten rat sarcoma viral oncogene homolog (*KRAS*) mutation, rearranged during transfection (*RET*) rearrangement, C-ros oncogene 1 receptor tyrosine kinase (*ROS1*) rearrangement, v-raf murine sarcoma viral oncogene homolog B1 (*BRAF*) mutation, and human epidermal growth factor receptor 2 (*HER2*) mutation, among others, were simultaneously detected. We stratified the clinical, CT imaging, and pathological features according to each gene mutation.

Statistical analysis

SPSS 24.0 statistical software (IBM Corp., Armonk, NY, USA) was used for statistical analysis, and GraphPad Prism 8.0 (GraphPad Software) was used to draw a forest map of the results of binary logistic regression analysis. A two-tailed P value of <0.05 was considered statistically significant.

The continuous data (such as age, NS_{max}, etc.) are expressed as the mean ± standard deviation (SD), and a *t*-test or one-way analysis of variance was used for comparison between groups. Categorical variables were analyzed with

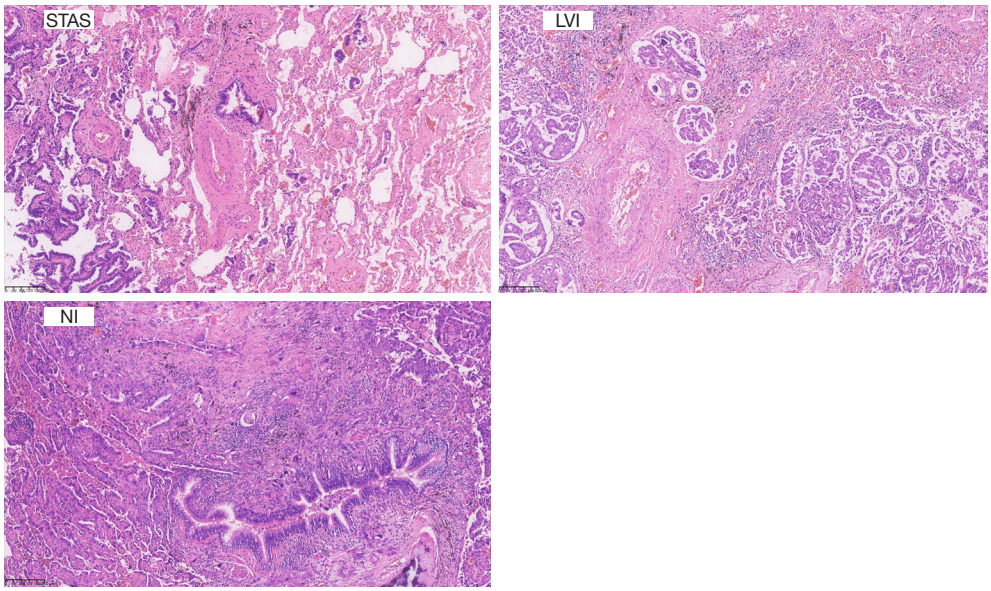

Figure 4 Common pathological features of IAC (hematoxylin-eosin staining, 10× magnification power). STAS, spread through air spaces; LVI, lymphovascular invasion; NI, nerve invasion; IAC, invasive adenocarcinoma.

the chi-squared test or Fisher exact test. The variables with statistical significance (P<0.05) in univariate statistical analysis and variables screened according to professional knowledge were selected to construct a binary or multivariate logistic regression equation for further binary or multivariate logistic regression analysis. The CT_m data is presented as mean (minimum, maximum).

According to the positive results of binary logistic regression analysis of binary continuous variables, the receiver operating characteristic (ROC) curve was drawn to evaluate and determine the optimal diagnostic threshold.

Results

There was no missing outcome data in this study.

There were 190 patients with pulmonary nodules enrolled, including 137 cases of malignant pulmonary nodules (72.11%) and 53 cases of benign pulmonary nodules (27.89%). Among the malignant pulmonary nodules, there were 132 cases of adenocarcinoma (96.35%), 1 case of squamous cell carcinoma, 3 cases of metastases, and 1 case of lymphoepithelial carcinoma. And among the 53 benign pulmonary nodules, 27 cases were infectious lesions (10 cases of fungal infection, 6 cases of inflammatory lesions, 3 cases of tuberculosis, 3 cases of organizing pneumonia, 5 cases of granuloma), 4 cases of pulmonary sclerosing cell tumor, 5 cases of hamartoma, 4 cases of collagen fiber nodules, 1 case of intrapulmonary lymph node, 12 cases of others.

Among the 132 patients with nodular lung adenocarcinoma, 93 cases were GGN (70.45%) and 39 cases were SN (29.55%) according to the density of pulmonary nodule; moreover, regarding the postoperative pathological types, there were 9 cases of AAH/AIS (6.82%), 20 cases of MIA (15.15%), and 103 cases of IAC (78.03%). Among the 103 patients with IAC, 45 had LPA (43.69%), 48 had APA/PPA (46.60%), and 10 cases had MPA/SPA/IMA (9.71%).

Differential analysis of the clinical and CT imaging features between benign and malignant pulmonary nodules

Univariate statistical analysis of the clinical and CT imaging features between benign and malignant pulmonary nodules

The results of univariate statistical analysis (*Table 1*) showed that malignant pulmonary nodules were more common in women and nonsmokers, CT signs were mostly multiple GGNs (55/137, 40.15%) and pleural retraction, and the NS_{max} of malignant nodules was larger than that of benign nodules. These differences were all statistically significant (P<0.05).

Table 1 Comparative analysis of clinical and CT imaging features between malignant pulmonary nodules and benign pulmonary nodules

Characteristics	Malignant (n=137)	Benign (n=53)	t/χ^2 value	P value
Age (years), mean ± SD	55.39±10.698	52.26±11.675	1.759	0.08
Gender, n			39.273	<0.001*
Female	95	23		
Male	42	30		
Smoking, n			8.956	0.003*
Ever or current	20	18		
Never	117	35		
NS_{max} (cm), mean ± SD	1.563±0.6000	1.338±0.4817	2.689	0.008*
GGN number, n			10.821	0.001*
Solitary	82	45		
Multiple	55	8		
GGN density, n			25.084	<0.001*
pGGN	42†	9†		
mGGN	51†	6†		
SN	44‡	38‡		
GGN site, n			6.460	0.17
RUL	48	12		
RML	8	4		
RLL	21	14		
LUL	41	12		
LLL	19	11		
Pleural retraction sign, n			6.798	0.009*
Yes	50	9		
No	87	44		
Lobulation sign, n			0.760	0.38
Yes	34	10		
No	103	43		
Spiculation sign, n			0.791	0.37
Yes	37	11		
No	100	42		
Vacuole sign, n			0.520	0.47
Yes	42	9		
No	51	6		
Air bronchogram sign, n			1.124	0.29
Yes	21	5		
No	116	38		

*, P<0.05; †, ‡, labeling symbols, that is, labeling the same group, there is no statistical difference between the groups (P>0.05), labeling different groups, there is statistical significance between the groups (P<0.05). CT, computed tomography; SD, standard deviation; NS_{max}, maximum diameter of nodule size; GGN, ground-glass nodule; pGGN, pure ground-glass nodule; mGGN, mixed ground-glass nodule; SN, solid nodule; RUL, right upper lobe; RML, right middle lobe; RLL, right lower lobe; LUL, left upper lobe; LLL, left lower lobe.

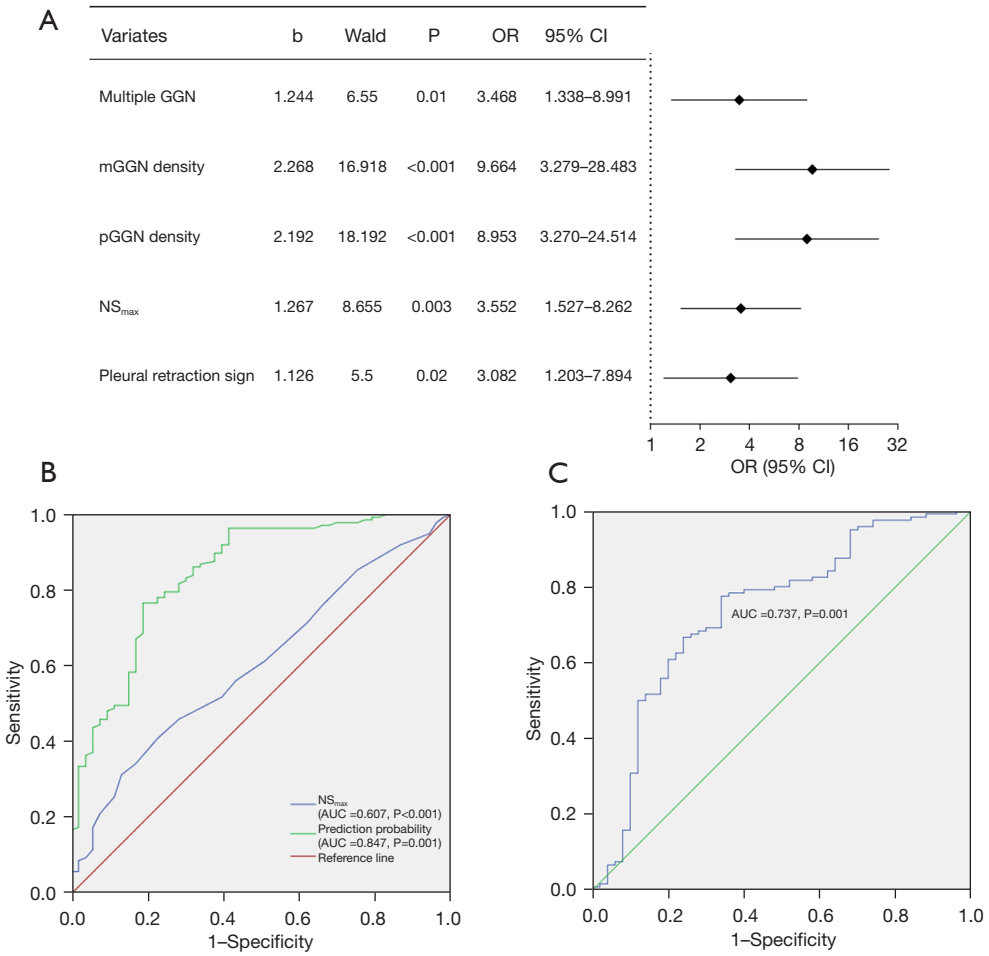

Figure 5 Analysis of CT imaging features between benign pulmonary nodules and malignant pulmonary nodules. (A) Forest plot of binary logistic regression analysis of CT imaging features of malignant pulmonary nodules. (B) ROC curves of multi-index combined diagnosis and NS_{max}. (C) ROC curve of CT_m between malignant pulmonary nodules and benign pulmonary nodules. b, regression coefficient; OR, odds ratio; CI, confidence interval; GGN, ground-glass nodule; mGGN, mixed ground-glass nodule; pGGN, pure ground-glass nodule; NS_{max}, maximum diameter of nodule size; AUC, area under the ROC curve; ROC, receiver operating characteristic; CT, computed tomography; CT_m, mean computed tomography.

Multivariate statistical analysis of clinical and CT imaging features between benign and malignant pulmonary nodule

Gender, smoking, GGN number, GGN density, NS_{max}, and pleural retraction sign were used to construct a binary logistic regression equation for multivariate statistical analysis. The results (*Figure 5A*) indicated that the CT signs of malignant pulmonary nodules were multiple GGNs [odds ratio (OR), 3.468; 95% confidence interval (CI): 1.338–8.991] and pleural retraction (OR, 3.083; 95% CI: 1.203–7.894), and the NS_{max} of malignant nodules was larger than that of benign nodules (OR, 3.552; 95% CI: 1.527–8.262). The area under the ROC curve (AUC) of the multi-index, combined diagnosis was 0.847 (*Figure 5B*).

Differential analysis of CT_m value between malignant pulmonary nodules and benign pulmonary nodules

The CT_m value of malignant pulmonary nodules was significantly lower than that of benign nodules (*Table 2*), and the AUC was 0.737 (*Figure 5C*). The corresponding maximum Youden index was 0.435, and the optimal diagnostic threshold of CT_m between malignant pulmonary nodules and benign nodules was –119.94 HU.

Table 2 Comparative analysis of CT_m value between malignant pulmonary nodules and benign pulmonary nodules

Characteristics	Malignant (n=120)	Benign (n=50)	*t* value	P value
CT_m value (HU)	−382.1936 (−741.80, 43.40)	−173.4452 (−738.60, 85.33)	−5.249	<0.001*

The CT_m data are presented as mean (minimum, maximum). *, P<0.05. CT_m, mean computed tomography.

Differential analysis of the clinical, CT imaging, and postoperative pathological features of each nodular lung adenocarcinoma subgroup

Differential analysis of the clinicopathological and CT imaging features between ground-glass nodular lung adenocarcinoma and solid nodular lung adenocarcinoma

Univariate statistical analysis of the clinical, CT imaging, and postoperative pathological type between ground-glass nodular lung adenocarcinoma and solid nodular lung adenocarcinoma

The results of univariate statistical analysis (*Table 3*) indicated that compared with those with ground-glass nodular lung adenocarcinoma (age, 53.85±11.045 years), the patients with solid nodular lung adenocarcinoma were relatively older (age, 59.74±8.952 years). Moreover, solid nodular lung adenocarcinoma had a larger NS_{max}; more commonly showed pleural retraction sign, lobulation sign, and spiculation signs on chest CT; and had a higher proportion of IAC. These differences were all statistically significant (P<0.05).

Multivariate statistical analysis of the clinicopathological and CT imaging features between ground-glass nodular lung adenocarcinoma and solid nodular lung adenocarcinoma

Age, gender, NS_{max}, pleural retraction sign, lobulation sign, spiculation sign, and postoperative pathological type were used to construct a binary logistic regression equation for multivariate statistical analysis. The results (*Figure 6A*) indicated that age, gender, lobulation sign, and spiculation sign were all positive factors for solid nodular lung adenocarcinoma. In other words, solid nodular lung adenocarcinoma was more common in women (OR, 3.662; 95% CI: 1.066–12.577) and older adults (OR, 1.061; 95% CI: 1.007–1.119) and more frequently showed lobulation sign (OR, 4.957; 95% CI: 1.714–14.337) and spiculation sign (OR, 8.214; 95% CI: 2.740–24.621) in chest CT. The AUC of the multi-index, combined diagnosis was 0.877 (*Figure 6B*).

Differential analysis of CT_m value between ground-glass nodular lung adenocarcinoma and solid nodular lung adenocarcinoma

The CT_m value of ground-glass nodular lung adenocarcinoma was significantly lower than that of solid nodular lung adenocarcinoma (*Figure 7A*, *Table 4*), the AUC was 0.9551 (*Figure 7B*), and the optimal diagnostic threshold of CT_m was −267.5 HU.

Differential analysis of the clinical and CT imaging features among AAH/AIS, MIA, and IAC

Univariate statistical analysis of the clinical and CT imaging features among AAH/AIS, MIA, and IAC

The results of univariate statistical analysis (*Table 5*) suggested that compared with MIA, IAC is more common among males and older adults. SN, pleural retraction sign, spiculation sign, air bronchogram sign were more common in chest CT signs of IAC, and the NS_{max} of IAC was larger. These differences were all statistically significant (P<0.05).

It should be mentioned that due to the small sample size of patients with AAH/AIS and MIA and the air bronchogram sign of both subgroups being 0, AAH/AIS and MIA were combined into a single group (AAH/AIS + MIA) to improve the efficiency of the chi-squared test through increasing the sample size.

Multivariate statistical analysis of the clinical and CT imaging features among AAH/AIS, MIA, and IAC

Age, gender, GGN density, NS_{max}, pleural retraction sign, spiculation sign, and air bronchogram sign were included to construct a multivariate logistic regression equation for multivariate statistical analysis. The results (*Table 6*) indicated that the NS_{max} of IAC was significantly higher than that of MIA (OR, 6.306; 95% CI: 1.191–33.400) and AAH/AIS (OR, 189.539; 95% CI: 4.720–7,610.476), with the AUCs being 0.794 and 0.866 (*Figure 8A,8B*), respectively, and the corresponding maximum Youden index values being 0.709 and 0.609, respectively. The diagnostic threshold of NS_{max} for IAC was 1.35 cm.

In addition, the results indicated that the age of patients with AAH/AIS was relatively higher than that of those with

Table 3 Comparative analysis of clinicopathological and CT imaging features between ground-glass nodular lung adenocarcinoma and solid nodular lung adenocarcinoma

Characteristics	Ground-glass type (n=93)	Solid type (n=39)	t/χ^2 value	P value
Age (years), mean ± SD	53.85±11.045	59.74±8.952	2.949	0.004*
Gender, n			1.648	0.20
Female	61	30		
Male	32	9		
Smoking, n			0.234	0.63
Ever/current	15	5		
Never	78	34		
Personal and family history of cancer, n			–	>0.99
Yes	5	2		
No	88	37		
GGN number, n			0.630	0.43
Solitary	57	21		
Multiple	36	18		
GGN site, n			1.763	0.78
RUL	36	12		
RML	4	3		
RLL	12	7		
LUL	29	11		
LLL	12	6		
Pleural retraction sign, n	27	21	7.311	0.007*
Lobulation sign, n	13	20	20.393	<0.001*
Spiculation sign, n	12	23	29.932	<0.001*
Vacuole sign, n	16	8	0.202	0.65
Air bronchogram sign, n	16	4	1.032	0.31
NS_{max} (cm), mean ± SD	1.438±0.5503	1.887±0.6161	4.132	<0.001*
Postoperative pathological type, n			13.002	0.001*
AAH/AIS	9†	0‡		
MIA	19†	1‡		
IAC	65†	38‡		

*, P<0.05; †, ‡, labeling symbols, that is, labeling the same group, there is no statistical difference between the groups (P>0.05), labeling different groups, there is statistical significance between the groups (P<0.05). CT, computed tomography; SD, standard deviation; GGN, ground-glass nodule; RUL, right upper lobe; RML, right middle lobe; RLL, right lower lobe; LUL, left upper lobe; LLL, left lower lobe; NS_{max}, maximum diameter of nodule size; AAH, atypical adenomatous hyperplasia; AIS, adenocarcinoma in situ; MIA, minimally invasive adenocarcinoma; IAC, invasive adenocarcinoma.

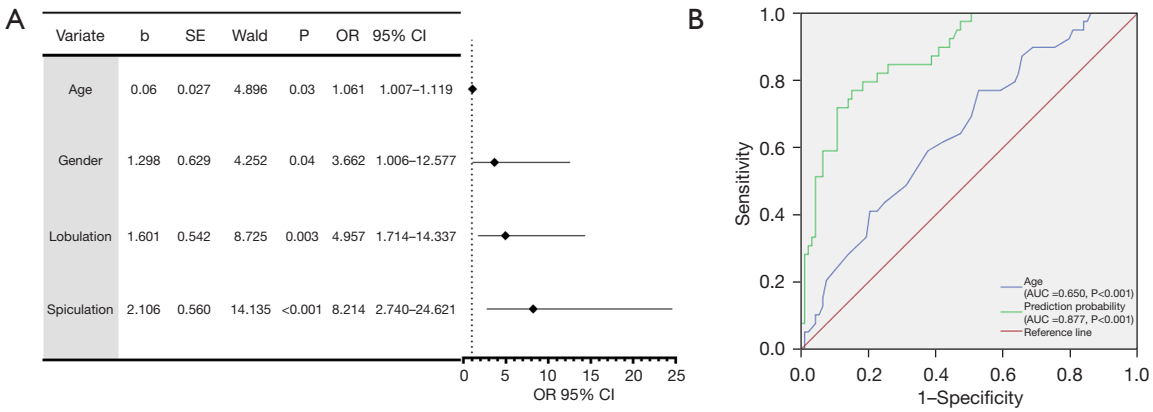

Figure 6 Analysis of the clinical, CT imaging features between ground-glass nodular lung adenocarcinoma and solid nodular lung adenocarcinoma. (A) Forest plot of binary logistic regression analysis of solid nodular lung adenocarcinoma. (B) ROC curves of multi-index combined diagnosis and age. b, regression coefficient; SE, standard error; OR, odds ratio; CI, confidence interval; AUC, area under the ROC curve; ROC, receiver operating characteristic; CT, computed tomography.

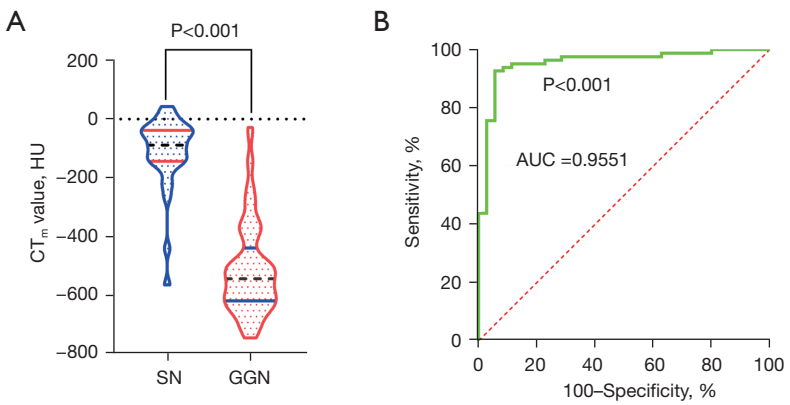

Figure 7 Comparative analysis of CT_m values between ground-glass nodular adenocarcinoma and solid nodular adenocarcinoma. (A) Violin plot of CT_m values between ground-glass nodular adenocarcinoma and solid nodular adenocarcinoma; (B) ROC curve of CT_m value between ground-glass nodular adenocarcinoma and solid nodular lung adenocarcinoma. CT_m, mean computed tomography; HU, Hounsfield units; SN, solid nodule; GGN, ground-glass nodule; AUC, area under the ROC curve; ROC, receiver operating characteristic.

Table 4 Comparative analysis of CT_m value between ground-glass nodular lung adenocarcinoma and solid nodular lung adenocarcinoma

Characteristics	Ground-glass type (n=82)	Solid type (n=35)	*t* value	P value
CT_m value (HU)	−511.49 (−741.80, −27.3)	−109.34 (−561.7, 43.4)	−13.677	<0.001*

The CT_m data are presented as mean (minimum, maximum). *, P<0.05. CT_m, mean computed tomography.

Table 5 Comparative analysis of clinical and CT imaging features among AAH/AIS, MIA, and IAC

Characteristics	AAH/AIS (n=9)	MIA (n=20)	IAC (n=103)	F/χ^2 value	P value
Age (years), mean ± SD	55.22±15.514†,‡	48.35±8.999‡	57.03±10.145†	5.835	0.004*
Gender, n				12.072	0.002*
Female	6†,‡	13‡	31†		
Male	3†,‡	7‡	72†		
Smoking, n				0.426	0.90
Ever/current	1	2	17		
Never	8	18	86		
Personal and family history of cancer, n				1.278	0.59
Yes	0	2	5		
No	9	18	98		
GGN number, n				0.796	0.67
Solitary	6	13	58		
Multiple	3	7	45		
GGN density, n				15.910	0.002*
pGGN	5†,‡	11‡	26†		
mGGN	4†	8†	39†		
SN	0†,‡	1‡	38†		
GGN site, n				6.242	0.58
RUL	1	10	37		
RML	1	0	6		
RLL	2	3	14		
LUL	3	5	32		
LLL	2	2	14		
Chest CT features, n					
Pleural retraction sign	2†,‡	2‡	44†	8.582	0.01*
Lobulation sign	0	3	30	4.680	0.09
Spiculation sign	0†,‡	1‡	34†	10.574	0.005*
Vacuole sign	0	4	20	1.798	0.45
Air bronchogram sign	0†	0†	20‡	–	0.007*
NS_{max} (cm), mean ± SD	0.9778±0.25386†	1.1250±0.36974†	1.7087±0.59096‡	31.169	<0.001*

*, P<0.05; †, ‡, labeling symbols, that is, labeling the same group, there is no statistical difference between the groups (P>0.05), labeling different groups, there is statistical significance between the groups (P<0.05). CT, computed tomography; AAH, atypical adenomatous hyperplasia; AIS, adenocarcinoma in situ; MIA, minimally invasive adenocarcinoma; IAC, invasive adenocarcinoma; SD, standard deviation; GGN, ground-glass nodule; pGGN, pure ground-glass nodule; mGGN, mixed ground-glass nodule; SN, solid nodule; RUL, right upper lobe; RML, right middle lobe; RLL, right lower lobe; LUL, left upper lobe; LLL, left lower lobe; NS_{max}, maximum diameter of nodule size.

Table 6 Multivariate logistic regression analysis of clinical and CT imaging features among AAH/AIS, MIA, and IAC

Subtype	b	SE	Wald	P	OR (95% CI)
AAH/AIS					
Age (*vs*. MIA)	0.136	0.058	5.460	0.02	1.145 (1.022–1.283)
IAC					
NS_{max} (*vs*. MIA)	1.842	0.851	4.688	0.03	6.306 (1.191–33.400)
NS_{max} (*vs*. AAH/AIS)	5.245	1.884	7.749	0.005	189.539 (4.720–7,610.476)

CT, computed tomography; AAH, atypical adenomatous hyperplasia; AIS, adenocarcinoma in situ; MIA, minimally invasive adenocarcinoma; IAC, invasive adenocarcinoma; b, regression coefficient; SE, standard error; OR, odds ratio; CI, confidence interval; NS_{max}, maximum diameter of nodule size.

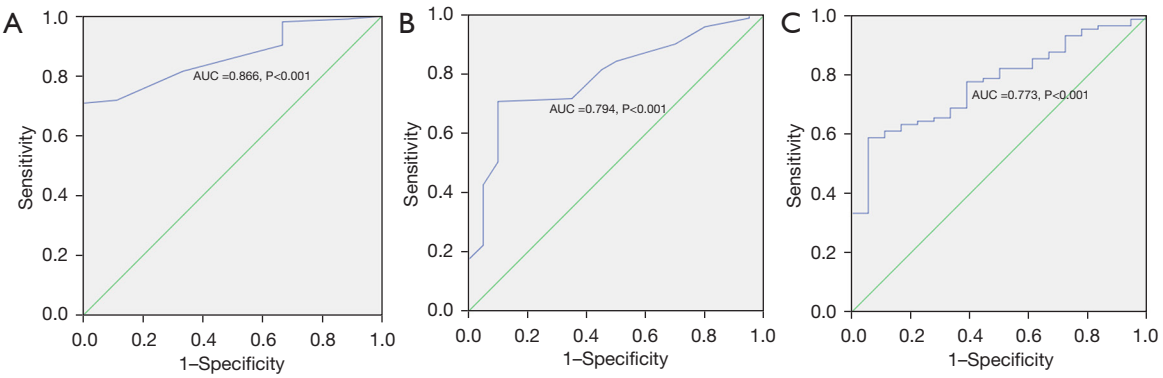

Figure 8 Analysis of the CT imaging feature among AAH/AIS, MIA, and IAC. (A) ROC curve of NS_{max} between IAC and AAH/AIS. (B) ROC curve of NS_{max} between IAC and MIA. (C) ROC curve of CT_m value between MIA and IAC. AUC, area under the ROC curve; ROC, receiver operating characteristic; CT, computed tomography; AAH, atypical adenomatous hyperplasia; AIS, adenocarcinoma in situ; MIA, minimally invasive adenocarcinoma; IAC, invasive adenocarcinoma; NS_{max}, maximum diameter of nodule size; CT_m, mean computed tomography.

Table 7 Comparative analysis of CT_m values among AAH/AIS, MIA, and IAC

Characteristics	AAH/AIS (n=9)	MIA (n=18)	IAC (n=90)	*F* value	P value
CT_m value (HU)	−591.7078† (−716.10, −268.50)	−557.7111† (−731.80, −147.40)	−337.8340‡ (−741.80, 3.40)	20.870	<0.001

The CT_m data are presented as mean (minimum, maximum). †, ‡, labeling symbols, that is, labeling the same group, there is no statistical difference between the groups (P>0.05), labeling different groups, there is statistical significance between the groups (P<0.05). CT_m, mean computed tomography; AAH, atypical adenomatous hyperplasia; AIS, adenocarcinoma in situ; MIA, minimally invasive adenocarcinoma; IAC, invasive adenocarcinoma.

MIA, but the P value of the ROC curve test was 0.157, so the difference was not statistically significant.

Differential analysis of CT_m value among AAH/AIS, MIA, and IAC

The CT_m value of IAC was significantly higher than that of MIA (*Table 7*), with an AUC of 0.773 (*Figure 8C*). The corresponding maximum Youden index value was 0.533, and the optimal diagnostic threshold of CT_m between MIA and IAC was −460.75 HU.

Differential analysis of the clinicopathological and CT imaging features among LPA, APA/PPA, and MPA/SPA/IMA

Univariate statistical analysis of the clinicopathological and CT imaging features among LPA, APA/PPA, and MPA/SPA/IMA

The results of univariate statistical analysis (*Tables 8*,*9*) suggested that compared to those with LPA and APA/PPA, the patients with MPA/SPA/IMA were relatively older,

Table 8 Comparative analysis of clinicopathological features of the IAC subgroups

Characteristics	LPA (n=45)	APA/PPA (n=48)	MPA/SPA/IMA (n=10)	F/χ^2 value	P value
Age (years), mean ± SD	56.62±11.021†	55.73±9.437†	65.10±5.021‡	3.792	0.03*
Gender, n				3.283	0.19
Female	30	37	5		
Male	15	11	5		
Smoking, n				10.520	0.005*
Ever/current	8†,‡	4‡	5†		
Never	37†,‡	44‡	5†		
Personal and family history of cancer, n				0.392	>0.99
Yes	2	3	0		
No	43	45	10		
pT, n				9.512	0.14
T1a	23	18	2		
T1b	18	18	4		
T1c	3	5	2		
T2	1	7	2		
pN, n				3.481	0.14
N0	43	46	8		
N1–2	2	2	2		
STAS, n				8.950	0.01*
Positive	14†	24†,‡	8‡		
Negative	31†	24†,‡	2‡		
LVI, n				8.584	0.008*
Positive	2†	4†	4‡		
Negative	43†	44†	6‡		
NI, n				4.932	0.10
Positive	0	0	1		
Negative	45	48	9		

*, P<0.05; †, ‡, labeling symbols, that is, labeling the same group, there is no statistical difference between the groups (P>0.05), labeling different groups, there is statistical significance between the groups (P<0.05). IAC, invasive adenocarcinoma; LPA, lepidic-predominant adenocarcinoma; APA, acinar-predominant adenocarcinoma; PPA, papillary-predominant adenocarcinoma; MPA, micropapillary-predominant adenocarcinoma; SPA, solid-predominant adenocarcinoma; IMA, invasive mucinous adenocarcinoma; SD, standard deviation; STAS, spread through air spaces; LVI, lymphovascular invasion; NI, nerve invasion.

Table 9 Comparative analysis of CT imaging features of the IAC subgroups

Characteristics	LPA (n=45)	APA/PPA (n=48)	MPA/SPA/IMA (n=10)	F/χ^2 value	P value
GGN number, n				0.252	0.88
Solitary	25	28	5		
Multiple	20	20	5		
GGN density, n				25.223	<0.001*
pGGN	17†	9†	0†		
mGGN	22†	16†	1†		
SN	6†	23‡	9§		
GGN site, n				7.562	0.44
RUL	16	16	5		
RML	5	1	0		
RLL	4	10	0		
LUL	14	15	3		
LLL	6	6	2		
NS_{max} (cm), mean ± SD	1.664±0.6267	1.723±0.6092	1.810±0.3281	0.280	0.76
Pleural retraction sign, n				4.852	0.09
Yes	15	22	7		
No	30	26	3		
Lobulation sign, n				14.450	0.001*
Yes	6†	17‡	7‡		
No	39†	31‡	3‡		
Spiculation sign, n				4.611	0.10
Yes	10	19	5		
No	35	29	5		
Vacuole sign, n				2.981	0.23
Yes	12	6	3		
No	33	42	8		
Air bronchogram sign, n				2.697	0.26
Yes	10	10	0		
No	35	38	10		

*, P<0.05; †, ‡, §, labeling symbols, that is, labeling the same group, there is no statistical difference between the groups (P>0.05), labeling different groups, there is statistical significance between the groups (P<0.05). CT, computed tomography; IAC, invasive adenocarcinoma; LPA, lepidic-predominant adenocarcinoma; APA, acinar-predominant adenocarcinoma; PPA, papillary-predominant adenocarcinoma; MPA, micropapillary-predominant adenocarcinoma; SPA, solid-predominant adenocarcinoma; IMA, invasive mucinous adenocarcinoma; GGN, ground-glass nodule; pGGN, pure ground-glass nodule; mGGN, mixed ground-glass nodule; SN, solid nodule; RUL, right upper lobe; RML, right middle lobe; RLL, right lower lobe; LUL, left upper lobe; LLL, left lower lobe; NS_{max}, maximum diameter of nodule size; SD, standard deviation.

Table 10 Multivariate logistic regression analysis of the clinical, CT imaging, and pathological features of the IAC subgroup

Subtype	b	SE	Wald	P	OR (95% CI)
LPA (*vs*. APA/PPA)					
pGGN	1.441	0.632	5.194	0.02	4.224 (1.223–14.585)
mGGN	1.833	0.753	5.923	0.02	6.252 (1.429–27.358)

CT, computed tomography; IAC, invasive adenocarcinoma; b, regression coefficient; SE, standard error; OR, odds ratio; CI, confidence interval; LPA, lepidic-predominant adenocarcinoma; pGGN, pure ground-glass nodule; mGGN, mixed ground-glass nodule; APA, acinar-predominant adenocarcinoma; PPA, papillary-predominant adenocarcinoma.

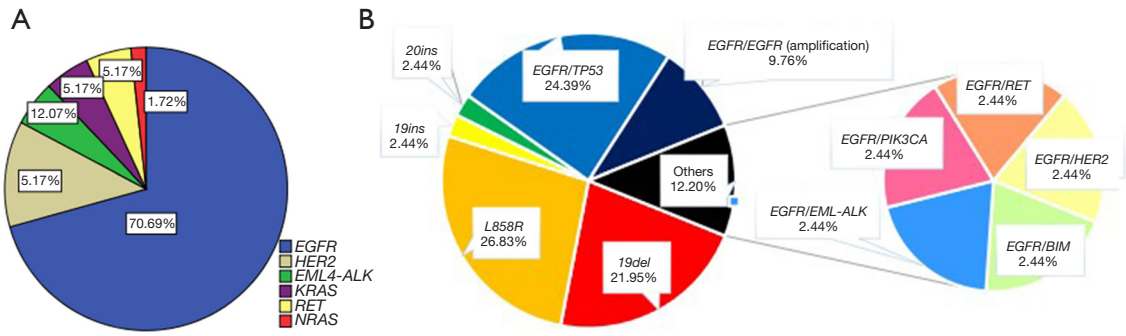

Figure 9 The genetic profile of IAC. (A) Genetic alterations in IAC. (B) *EGFR* mutational spectrum. *EGFR*, epidermal growth factor receptor; *HER2*, human epidermal growth factor receptor 2; *EML-ALK*, echinoderm microtubule-associated protein like 4-anaplastic lymphoma kinase; *KRAS*, Kirsten rat sarcoma viral oncogene homolog; *RET*, rearranged during transfection; *NRAS*, neuroblastoma RAS viral oncogene homolog; *TP53*, tumor protein p53; *BIM*, B-cell lymphoma 2 interacting mediator of cell death; *PIK3CA*, phosphatidylinositol-4,5-bisphosphate 3-kinase catalytic subunit alpha; IAC, invasive adenocarcinoma.

with STAS and LVI being common in MPA/SPA/IMA; the proportion of SN was the highest in high-grade pathological subtypes, followed by medium-grade pathological subtypes, and the lowest in low-grade pathological subtypes; the lobulation sign was more common in CT images of medium- and high-grade pathological subtypes. These differences were all statistically significant (P<0.05).

Multivariate statistical analysis of the clinicopathological and CT imaging features among LPA, APA/PPA, and MPA/SPA/IMA

Age, smoking, GGN density, pleural retraction sign, lobulation sign, STAS, LVI, and NI were used to construct a multivariate logistic regression equation for multivariate statistical analysis. The results (*Table 10*) indicated that chest CT signs of LPA were mostly pure GGNs (pGGNs; OR, 6.252; 95% CI: 1.429–27.358) or mixed GGNs (mGGNs; OR, 4.224; 95% CI: 1.223–14.585).

The gene mutation profile of IAC and its clinical, CT imaging, and pathological features

The recommended NSCLC targeted genes were simultaneously detected with NGS in 58 postoperative lung tissue samples of IAC. The total gene mutation rate was 94.83% (55/58), and the *EGFR* mutation rate was 70.69% (41/58), as shown in *Figure 9A,9B*.

The clinical, CT imaging, and pathological features of the *EGFR* mutation

The results of univariate analysis (*Table 11*) showed that the *EGFR* mutation rate in APA/PPA was significantly higher than that in MPA/SPA/IMA (P<0.05), while there was no significant difference in the mutation rate between APA/PPA and LPA (P>0.05).

GGN density and pathological grade were used to

Table 11 Comparative analysis of clinicopathological and CT imaging features of *EGFR* mutation in IAC

Characteristics	*EGFR*		χ^2 value	P value
	Wild type (n=17)	Mutation (n=41)		
Gender, n			0.107	0.74
Male	6	11		
Female	11	30		
Smoking, n			1.366	0.24
Ever/current	6	7		
Never	11	34		
GGN density, n			6.070	0.048*
Mix	3†	16†		
Pure	8†	7†		
Solid	6†	18†		
Pleural retraction sign, n			0.598	0.44
Yes	6	19		
No	11	22		
Lobulation sign, n			0.477	0.49
Yes	7	13		
No	10	28		
Spiculation sign, n			0.274	0.60
Yes	5	15		
No	12	26		
Vacuole sign, n			0.000	>0.99
Yes	3	8		
No	14	33		
Air bronchogram sign, n			0.108	0.74
Yes	2	8		
No	15	33		
Pathological grade, n			9.300	0.007*
LPA	7†,‡	16†,‡		
APA/PPA	5†	24†		
MPA/SPA/IMA	5‡	1‡		
pT, n			3.408	0.31
T1a	10	15		
T1b	4	18		
T1c	2	3		
T2	1	5		

Table 11 (*continued*)

Table 11 (*continued*)

Characteristics	*EGFR*		χ^2 value	P value
	Wild type (n=17)	Mutation (n=41)		
pN, n			0.000	>0.99
N0	16	38		
N1–2	1	3		
STAS, n			0.949	0.33
Positive	9	16		
Negative	8	25		
LVI, n			0.000	>0.99
Positive	2	5		
Negative	15	36		

*, P<0.05; †, ‡, labeling symbols, that is, labeling the same group, there is no statistical difference between the groups (P>0.05), labeling different groups, there is statistical significance between the groups (P<0.05). CT, computed tomography; *EGFR*, epidermal growth factor receptor; IAC, invasive adenocarcinoma; GGN, ground-glass nodule; LPA, lepidic-predominant adenocarcinoma; APA, acinar-predominant adenocarcinoma; PPA, papillary-predominant adenocarcinoma; MPA, micropapillary-predominant adenocarcinoma; SPA, solid-predominant adenocarcinoma; IMA, invasive mucinous adenocarcinoma; STAS, spread through air spaces; LVI, lymphovascular invasion.

Table 12 Binary logistic regression analysis of *EGFR* mutation in IAC

Variate	b	SE	Wald	P	OR (95% CI)
mGGN (*vs*. pGGN)	2.174	0.906	5.757	0.02	8.794 (1.489–51.933)
SN (*vs*. pGGN)	2.558	1.066	5.756	0.02	12.912 (1.597–104.383)
LPA (*vs*. MPA/SPA/IMA)	3.645	1.433	6.469	0.01	38.265 (2.307–634.596)
APA/PPA (*vs*. MPA/SPA/IMA)	4.024	1.340	9.016	0.003	55.925 (4.045–773.284)

EGFR, epidermal growth factor receptor; IAC, invasive adenocarcinoma; b, regression coefficient; SE, standard error; OR, odds ratio; CI, confidence interval; mGGN, mixed ground-glass nodule; SN, solid nodule; LPA, lepidic-predominant adenocarcinoma; APA, acinar-predominant adenocarcinoma; PPA, papillary-predominant adenocarcinoma; pGGN, pure ground-glass nodule; MPA, micropapillary-predominant adenocarcinoma; SPA, solid-predominant adenocarcinoma; IMA, invasive mucinous adenocarcinoma.

construct a binary logistic regression equation for multivariate statistical analysis. The results (*Table 12*) found that the *EGFR* mutation rates of mGGN (OR, 8.794; 95% CI: 1.489–51.933) and SN (OR, 12.912; 95% CI: 1.597–104.383) were significantly higher than that of pGGN, and the *EGFR* mutation rates of APA/PPA (OR, 55.925; 95% CI: 4.045–773.284) and LPA (OR, 38.265; 95% CI: 2.307–634.596) were significantly higher than that of MPA/SPA/IMA.

Further statistical analysis showed that there was no significant difference in the clinical, imaging, or pathological features of *EGFR* subgroup mutations (exon 19 deletion and L858R point mutation) (P>0.05). There was no T790M mutation found in the examined cases.

The clinical, CT imaging, and pathological features of HER2, KRAS, and other gene mutations

The results of univariate analysis (*Table 13*) showed that the *HER2* mutation rate of pGGNs was significantly higher than that of mGGNs while the mutation rate of *KRAS* in male smokers was significantly higher than that in female nonsmokers, with these differences all being statistically significant (P<0.05). However, no statistically significant results were found in the multivariate analysis through the construction of the binary logistic regression equation (P>0.05). There were no significant differences associated with the clinical, CT imaging, or pathological features of *EML-ALK*, *RET*, *ROS1*, and other gene fusion mutations (P>0.05).

Table 13 The positive results of the clinicopathological and CT imaging features of *KRAS* and *HER2* mutation in IAC

Characteristics	*KRAS*				*HER2*			
	Wild type (n=55)	Mutation (n=3)	χ^2 value	P value	Wild type (n=51)	Mutation (n=7)	χ^2 value	P value
GGN density, n			1.619	0.47			7.828	0.01*
Mix	17	2			19†	0†		
Pure	15	0			10‡	5‡		
Solid	23	1			22†,‡	2†,‡		
Gender, n			–	0.02*			0.239	0.63
Male	14	3			16	1		
Female	41	0			35	6		
Smoking, n			–	0.009*			0.004	0.95
Ever/current	10	3			12	1		
Never	45	0			39	6		

*, P<0.05; †, ‡, labeling symbols, that is, labeling the same group, there is no statistical difference between the groups (P>0.05), labeling different groups, there is statistical significance between the groups (P<0.05). CT, computed tomography; *KRAS*, Kirsten rat sarcoma viral oncogene homolog; *HER2*, human epidermal growth factor receptor 2; IAC, invasive adenocarcinoma; GGN, ground-glass nodule.

Disscussion

To our knowledge, adenocarcinoma is the most common histological subtype of NSCLC (15) and the main pathological type of malignant pulmonary nodules (12). In this study, the proportion of nodular lung adenocarcinoma was as high as 96.35% (132/137). In LDCT lung cancer screening, early lung cancer often manifests as GGNs, including pGGNs and mGGNs. It has been reported that persistent appearance of GGNs in the lungs is typically early nodular lung adenocarcinoma (10), such as AAH/AIS, MIA, and IAC.

Smoking is a widely recognized risk factor for lung cancer. However, in many Asian countries, especially in China, patients with nodular lung adenocarcinoma are mostly nonsmoking women (16), which may be closely related to the environmental particulate matter pollution (17), household smoke pollution (18), gender inheritance (19), and estrogen levels in women (20). It is reported that more than one-third of children and nonsmokers are exposed to smoking environments (21), and approximately 3% of the five billion people who are exposed to household air pollution live in China and India (22). Inherited genetic variations can also promote the occurrence and development of lung cancer, with the *EGFR* mutation being the most common genetic aberration that is present in nonsmoking females with nodular lung adenocarcinoma (23). Age is also an independent risk factor for lung cancer. More than 80% of patients with lung cancer in China are over 50 years old (24). In this study, the results of univariate statistical analysis indicated the following: malignant pulmonary nodules were more likely to occur in nonsmoking women; compared with those with ground-glass nodular lung adenocarcinoma, the patients with solid nodular lung adenocarcinoma were relatively older; and compared with those with MIA, patients with IAC were older and tended to be male. Further multivariate logistic regression analysis indicated that solid nodular lung adenocarcinoma was more common in women and relatively older people, which is consistent with the gender orientation and development process of lung adenocarcinoma.

With the increase in malignant nodule infiltration, the tumor cells invade the surrounding normal lung tissues. Chest CT often displays irregular margins such as lobulation sign, spiculation sign, and pleural retraction sign; moreover, when the tumor cells invade the wall of blood vessels and bronchi, the bronchioles are twisted and dilated, thus causing vacuole sign or air bronchogram sign to appear on chest CT (11). In this study, the results of univariate and multivariate statistical analyses suggested that pleural retraction sign was more common in malignant pulmonary nodules; compared with ground-glass nodular lung adenocarcinoma, solid nodular lung adenocarcinoma more

frequently showed lobulation sign and speculation sign.

Nodule size has a clear relationship with risk of malignancy (9), that is, the larger nodule, the higher the possibility of malignancy (25). The results of univariate and multivariate statistical analysis in this study indicated that the NS_{max} of IAC was significantly greater than that of MIA or AAH/AIS, with the corresponding AUCs being 0.794 and 0.866, respectively. The optimal NS_{max} value for differentiating IAC from IMA was calculated to be 1.35 cm. Considering the small sample size of AAH/AIS and MIA, it is impossible to further clarify the optimal NS_{max} value between them. Yue *et al.* (26) reported that the optimal NS_{max} value between MIA and IAC is 14.7 mm (sensitivity, 90%; specificity, 81%).

CT_m value is also an important predictor for the degree of invasion of nodular lung adenocarcinoma (27). With the incremental transition of AAH/AIS to MIA and IAC in pathological staging, the density of tumor cell components in the lesion respectively increases, and the CT value also increases accordingly (28). The results in our study suggested that the CT_m value of malignant pulmonary nodules was significantly lower than that of benign nodules, the AUC was 0.737, and the optimal CT_m value was –119.94 HU; the CT_m value of ground-glass nodular lung adenocarcinoma was significantly lower than that of solid nodular lung adenocarcinoma, the AUC was 0.9551, and the optimal diagnostic threshold of CT_m was –267.5 HU; the CT_m value of IAC was significantly higher than that of MIA and AAH/AIS, the corresponding AUC was 0.773 and 0.833, and the optimal CT_m value was –460.75 HU and –554.55HU, respectively. Therefore, we believe that the CT_m of IAC is between –460 and –120 HU, the CT_m of MIA is between –460 and –554.55 HU, while the CT_m <–460 HU can be considered to indicate AAH/AIS. Fu *et al.* (29) reported that the CT_m of imaging findings of pGGN among patients with AIS, MIA, or IAC was no difference, and believed that the measurement of CT_m for pGGN does not predict pathological subtypes because pGGN is essentially a lepidic component, and the CT value of a considerable part of the region is very low. Furthermore, owing to the lack of a unified standardized measurement method for the measurement of the CT_m value and the unavoidable interference of blood vessels, bronchi, and other factors in the measurement process, the accuracy of the measurement will be inconsistent. Thus, some authors (30) believe that the CT_m value has poor diagnostic efficacy for the degree of adenocarcinoma infiltration, and only NS_{max} can be used for this purpose.

The NELSON study (31) showed that up to 48.5% of patients with GGNs have multiple GGNs. The results of univariate and multivariate statistical analysis in our study showed that malignant nodules were mostly multiple GGNs (55/137, 40.15%. The nature of multiple GGNs may be satellite nodules (the same lobe, no systemic metastasis), multiple primary lung cancer (different lobes, no N2–N3 lymph node involvement or systemic metastasis), or pulmonary metastases (different lobes, N2–N3 lymph node involvement) (32). At present, it is believed that the pathological manifestations of most multiple GGNs are synchronous multisource early lung adenocarcinoma (33), this may be correlated with the high mutation rate of *EGFR* in lung adenocarcinoma (34), which has the characteristics of polyclonal origin and independent growth.

It is well known that patients with low-grade histopathological type (LPA) have the best prognosis, followed by those with the medium-grade histopathological types (APA and PPA), whereas patients with high-grade histopathological types (MPA and SPA) have the worst prognosis (14). Woo *et al.* (35) reported there was no significant difference in overall survival between IMA and MPA/SPA patients, so we classified IMA and MPA/SPA into one group. The results of univariate analysis in this study revealed that, compared with those with LPA or APA/PPA, the patients with MPA/SPA/IMA were relatively older; the proportion of SN in the CT signs of low-, medium-, and high-grade histopathological subtypes increased in turn; the lobulation sign was more common in the CT signs of medium and high-grade histopathological subtypes, which was consistent with the clinical imaging features of malignant SN in this study. Further multivariate logistic regression analysis showed that the CT signs of LPA were mostly pGGNs or mGGNs, which was in agreement with the previous report, in which the presence of GGNs on high-resolution CT was positively correlated with LPA (13). As an indispensable part of postoperative routine pathology of lung IAC, STAS, and LVI are correlated with a high risk of recurrence and poor clinical prognosis of early lung IAC (36), and STAS was reported to be more common in lung IAC with SNs (37). The results of univariate analysis in this study also indicated that STAS and LVI were more common in patients with MPA/SPA/IMA.

The progressive development of nodular lung adenocarcinoma is a dynamic process of multigene initiation and continuous modification, and AAH/AIS can gradually develop into MIA and IAC. In the study of Li *et al.* (38) classical *EGFR* mutations, such as exon 19

deletion and exon 21 L858R point mutation, tended to be associated with ground-glass composition on c-stage IA lung adenocarcinoma. In our study, the *EGFR* mutation rate of IAC was as high as 70.69% (41/58), and the *EGFR* mutation rate of mGGNs and SN was significantly higher than that of pGGNs (P<0.05). In other words, *EGFR* mutations were more common in pulmonary nodules with solid components. Moreover, the mutation rate of *EGFR* in APA/PPA and LPA was significantly higher than that in MPA/SPA/IMA (P<0.05), which was consistent with the study of Sun *et al.* (39). *ALK* fusion, known as diamond mutation, is a classic malignant SN mutation (40) and is often associated with driver mutation genes such as *RET* fusion and *ROS1* fusion. IMA is known to frequently harbor the *KRAS* mutation (41). In our study, the results of univariate statistical analysis showed that the *HER2* mutation rate of pGGNs was significantly higher than that of mGGNs while the *KRAS* mutation rate of male smokers was significantly higher than that of the female nonsmokers; no statistically significant difference was observed in *EML-ALK*, *ROS1*, and *RET* fusion mutations (P>0.05). With the rapid development of NGS technology, it is not uncommon for co-mutation of two or more genes to be detected in the same sample at a given time, especially in tumor-suppressor genes such as tumor protein p53 (*TP53*), which has become the core determinant of molecular and clinical heterogeneity of oncogene-driven lung cancer subsets (42). In this study, *EGFR/TP53* were the most common co-mutation (10/58, 17.2%). Kim *et al.* (43) reported that the *EGFR/TP53* co-mutation was associated with the efficacy of EGFR tyrosine kinase inhibitors (EGFR-TKIs) and found that *TP53* mutation was an independent poor prognostic factor.

This study focused on the clinical, CT imaging, and postoperative pathological features of different classifications of nodular lung adenocarcinoma, which has certain reference value for the differential diagnosis of nodular lung adenocarcinoma. However, some limitations to this study should be noted. Firstly, a retrospective study design was employed, and the pulmonary nodules enrolled were surgically resected and confirmed by pathology. This cannot represent the overall situation of pulmonary nodules, and a certain bias in case selection was inevitable. Secondly, we only included patients from a single center, the sample size was not sufficiently, and not all cases were tested with NGS. Therefore, our findings need to be further verified in a multicenter, prospective, randomized, large-sample study. Besides. there might have been errors in the measurement process of CT_m and NS_{max} of pulmonary nodules. Although the measured data were automatically calculated and generated using software, the CT values measured by manually sketching the ROIs are restricted by the location, size, shape, and other factors of the nodule, and interference from blood vessels, bronchi, etc., cannot be avoided. Due to these potential errors in the measurement, the repeatability of the results may be limited.

Conclusions

In conclusion, different classifications of nodular lung adenocarcinoma have their own clinicopathological and CT imaging features, and the latter is the main predictor.

Acknowledgments

The authors thank the participants and their families who actively participated in this study. The authors also thank their colleagues in the CT Imaging Department and Pathology Department of the First Affiliated Hospital of Gannan Medical University for their contributions to this study.

Funding: This work was supported by grants of the Doctoral Initiation Fund Project of the First Affiliated Hospital of Gannan Medical University (No. QD202310) and the Jiangxi Provincial Health Commission Science and Technology Plan Project (No. 202210951).

Footnote

Reporting Checklist: The authors have completed the STROBE reporting checklist. Available at https://jtd.amegroups.com/article/view/10.21037/jtd-24-510/rc

Data Sharing Statement: Available at https://jtd.amegroups.com/article/view/10.21037/jtd-24-510/dss

Peer Review File: Available at https://jtd.amegroups.com/article/view/10.21037/jtd-24-510/prf

Conflicts of Interest: All authors have completed the ICMJE uniform disclosure form (available at https://jtd.amegroups.com/article/view/10.21037/jtd-24-510/coif). The authors have no conflicts of interest to declare.

Ethical Statement: The authors are accountable for all aspects of the work in ensuring that questions related to the accuracy or integrity of any part of the work are

appropriately investigated and resolved. The study was conducted in accordance with the Declaration of Helsinki (as revised in 2013). The Ethics Committee of the First Affiliated Hospital of Gannan Medical University approved this retrospective study (No. LLSC-2022111603), and informed consent was taken from all the patients.

References

1. Sung H, Ferlay J, Siegel RL, et al. Global Cancer Statistics 2020: GLOBOCAN Estimates of Incidence and Mortality Worldwide for 36 Cancers in 185 Countries. CA Cancer J Clin 2021;71:209-49.
2. Zheng RS, Sun KX, Zhang SW, et al. Report of cancer epidemiology in China, 2015. Zhonghua Zhong Liu Za Zhi 2019;41:19-28.
3. Hong QY, Wu GM, Qian GS, et al. Prevention and management of lung cancer in China. Cancer 2015;121 Suppl 17:3080-8.
4. Carlos RC, Sicks JD, Chiles C, et al. Lung Cancer Screening in the National Cancer Institute Community Oncology Research Program: Availability and Service Organization. J Am Coll Radiol 2019;16:427-34.
5. Yang W, Qian F, Teng J, et al. Community-based lung cancer screening with low-dose CT in China: Results of the baseline screening. Lung Cancer 2018;117:20-6.
6. Yotsukura M, Asamura H, Motoi N, et al. Long-Term Prognosis of Patients With Resected Adenocarcinoma In Situ and Minimally Invasive Adenocarcinoma of the Lung. J Thorac Oncol 2021;16:1312-20.
7. Xu SJ, Chen RQ, Tu JH, et al. Effects of a ground-glass opacity component on the recurrence and survival of pathological stage IA3 lung adenocarcinoma: a multi-institutional retrospective study. Transl Lung Cancer Res 2023;12:1078-92.
8. Zheng C, Wang H, Liu Q, et al. Application effect of low-dose spiral CT on pulmonary nodules and its diagnostic value for benign and malignant nodules. Am J Transl Res 2023;15:256-63.
9. MacMahon H, Naidich DP, Goo JM, et al. Guidelines for Management of Incidental Pulmonary Nodules Detected on CT Images: From the Fleischner Society 2017. Radiology 2017;284:228-43.
10. Ren J, Wang Y, Liu C, et al. Correlation analysis of clinical, pathological, imaging and genetic features of ground-glass nodule featured lung adenocarcinomas between high-risk and non-high-risk individuals. Eur J Med Res 2023;28:478.
11. He W, Guo G, Du X, et al. CT imaging indications correlate with the degree of lung adenocarcinoma infiltration. Front Oncol 2023;13:1108758.
12. Wang Y, Huang Q, Li J. Analysis of Clinical and Pathological Features of Malignant Pulmonary Nodules. Altern Ther Health Med 2023;29:188-93.
13. Zhang P, Li T, Tao X, et al. HRCT features between lepidic-predominant type and other pathological subtypes in early-stage invasive pulmonary adenocarcinoma appearing as a ground-glass nodule. BMC Cancer 2021;21:1124.
14. Nicholson AG, Tsao MS, Beasley MB, et al. The 2021 WHO Classification of Lung Tumors: Impact of Advances Since 2015. J Thorac Oncol 2022;17:362-87.
15. Schabath MB, Cote ML. Cancer Progress and Priorities: Lung Cancer. Cancer Epidemiol Biomarkers Prev 2019;28:1563-79.
16. Zhang Y, Jheon S, Li H, et al. Results of low-dose computed tomography as a regular health examination among Chinese hospital employees. J Thorac Cardiovasc Surg 2020;160:824-831.e4.
17. Hill W, Lim EL, Weeden CE, et al. Lung adenocarcinoma promotion by air pollutants. Nature 2023;616:159-67.
18. Zhang T, Hoang PH, Wong JYY, et al. Distinct Genomic Landscape of Lung Adenocarcinoma from Household Use of Smoky Coal. Am J Respir Crit Care Med 2023;208:733-6.
19. Hu Z, Wu C, Shi Y, et al. A genome-wide association study identifies two new lung cancer susceptibility loci at 13q12.12 and 22q12.2 in Han Chinese. Nat Genet 2011;43:792-6.
20. Rodriguez-Lara V, Hernandez-Martinez JM, Arrieta O. Influence of estrogen in non-small cell lung cancer and its clinical implications. J Thorac Dis 2018;10:482-97.
21. Age-sex differences in the global burden of lower respiratory infections and risk factors, 1990-2019: results from the Global Burden of Disease Study 2019. Lancet Infect Dis 2022;22:1626-47.

22. Gordon SB, Bruce NG, Grigg J, et al. Respiratory risks from household air pollution in low and middle income countries. Lancet Respir Med 2014;2:823-60.
23. Han X, Fan J, Li Y, et al. Value of CT features for predicting EGFR mutations and ALK positivity in patients with lung adenocarcinoma. Sci Rep 2021;11:5679.
24. Long J, Zhai M, Jiang Q, et al. The incidence and mortality of lung cancer in China: a trend analysis and comparison with G20 based on the Global Burden of Disease Study 2019. Front Oncol 2023;13:1177482.
25. Cai Y, Chen T, Zhang S, et al. Correlation exploration among CT imaging, pathology and genotype of pulmonary ground-glass opacity. J Cell Mol Med 2023;27:2021-31.
26. Yue X, Liu S, Liu S, et al. HRCT morphological characteristics distinguishing minimally invasive pulmonary adenocarcinoma from invasive pulmonary adenocarcinoma appearing as subsolid nodules with a diameter of ≤3 cm. Clin Radiol 2018;73:411.e7-411.e15.
27. He S, Chen C, Wang Z, et al. The use of the mean computed-tomography value to predict the invasiveness of ground-glass nodules: A meta-analysis. Asian J Surg 2023;46:677-82.
28. Zhan Y, Peng X, Shan F, et al. Attenuation and Morphologic Characteristics Distinguishing a Ground-Glass Nodule Measuring 5-10 mm in Diameter as Invasive Lung Adenocarcinoma on Thin-Slice CT. AJR Am J Roentgenol 2019;213:W162-70.
29. Fu F, Zhang Y, Wang S, et al. Computed tomography density is not associated with pathological tumor invasion for pure ground-glass nodules. J Thorac Cardiovasc Surg 2021;162:451-459.e3.
30. Han L, Zhang P, Wang Y, et al. CT quantitative parameters to predict the invasiveness of lung pure ground-glass nodules (pGGNs). Clin Radiol 2018;73:504.e1-7.
31. Heuvelmans MA, Walter JE, Peters RB, et al. Relationship between nodule count and lung cancer probability in baseline CT lung cancer screening: The NELSON study. Lung Cancer 2017;113:45-50.
32. Ghosh S, Mehta AC, Abuquyyas S, et al. Primary lung neoplasms presenting as multiple synchronous lung nodules. Eur Respir Rev 2020;29:190142.
33. Zhang Y, Li G, Li Y, et al. Imaging Features Suggestive of Multiple Primary Lung Adenocarcinomas. Ann Surg Oncol 2020;27:2061-70.
34. Ren Y, Huang S, Dai C, et al. Germline Predisposition and Copy Number Alteration in Pre-stage Lung Adenocarcinomas Presenting as Ground-Glass Nodules. Front Oncol 2019;9:288.
35. Woo W, Yang YH, Cha YJ, et al. Prognosis of resected invasive mucinous adenocarcinoma compared with the IASLC histologic grading system for invasive nonmucinous adenocarcinoma: Surgical database study in the TKIs era in Korea. Thorac Cancer 2022;13:3310-21.
36. Akcam TI, Tekneci AK, Ergin TM, et al. Factors influencing postoperative recurrence of early-stage non-small cell lung cancer. Acta Chir Belg 2024;124:121-30.
37. Gu Y, Zheng B, Zhao T, et al. Computed Tomography Features and Tumor Spread Through Air Spaces in Lung Adenocarcinoma: A Meta-analysis. J Thorac Imaging 2023;38:W19-29.
38. Li M, Xi J, Sui Q, et al. Impact of a Ground-glass Opacity Component on c-Stage IA Lung Adenocarcinoma. Semin Thorac Cardiovasc Surg 2023;35:783-95.
39. Sun F, Xi J, Zhan C, et al. Ground glass opacities: Imaging, pathology, and gene mutations. J Thorac Cardiovasc Surg 2018;156:808-13.
40. Yoon HJ, Sohn I, Cho JH, et al. Decoding Tumor Phenotypes for ALK, ROS1, and RET Fusions in Lung Adenocarcinoma Using a Radiomics Approach. Medicine (Baltimore) 2015;94:e1753.
41. Matsui T, Sakakura N, Koyama S, et al. Comparison of Surgical Outcomes Between Invasive Mucinous and Non-Mucinous Lung Adenocarcinoma. Ann Thorac Surg 2021;112:1118-26.
42. Skoulidis F, Heymach JV. Co-occurring genomic alterations in non-small-cell lung cancer biology and therapy. Nat Rev Cancer 2019;19:495-509.
43. Kim Y, Lee B, Shim JH, et al. Concurrent Genetic Alterations Predict the Progression to Target Therapy in EGFR-Mutated Advanced NSCLC. J Thorac Oncol 2019;14:193-202.

Cite this article as: Zhong W, Zhang W, Dai L, Chen M. The clinical, radiological, postoperative pathological, and genetic features of nodular lung adenocarcinoma: a real-world single-center data. J Thorac Dis 2024;16(5):3228-3250. doi: 10.21037/jtd-24-510